Bingham fluid simulations using a physically consistent particle method

AUTHOR(S):

NEGISHI, Hideyo; KONDO, Masahiro; AMAKAWA, Hiroaki; OBARA, Shingo; KUROSE, Ryoichi

CITATION:

NEGISHI, Hideyo ...[et al]. Bingham fluid simulations using a physically consistent particle method. Journal of Fluid Science and Technology 2023, 18(4): JFST0035.

ISSUE DATE:

2023

URL:

http://hdl.handle.net/2433/286205

Bulletin of the JSME Vol.18, No.4, 2023
Journal of Fluid Science and Technology

Bingham fluid simulations using a physically consistent particle method

Hideyo NEGISHI*,***, Masahiro KONDO**, Hiroaki AMAKAWA*, Shingo OBARA*
and Ryoichi KUROSE***
*Japan Aerospace Exploration Agency
2-1-1 Sengen, Tsukuba, Ibaraki 305-8505, Japan
E-mail: negishi.hideyo@jaxa.jp
**National Institute of Advanced Industrial Science and Technology
Central 2, 1-1-1 Umezono, Tsukuba, Ibaraki 305-8568, Japan
***Department of Mechanical Engineering and Science, Kyoto University
Kyoto daigaku-katsura, Nishikyo-ku, Kyoto 615-8540, Japan

Received: 15 September 2023; Revised: 16 October 2023; Accepted: 1 November 2023

Abstract

The Bingham fluid simulation model was constructed and validated using a physically consistent particle method, i.e., the Moving Particle Hydrodynamics (MPH) method. When a discrete particle system satisfies the fundamental laws of physics, the method is asserted as physically consistent. Since Bingham fluids sometimes show solid-like behaviors, linear and angular momentum conservation is especially important. These features are naturally satisfied in the MPH method. To model the Bingham feature, the viscosity of the fluid was varied to express the stress-strain rate relation. Since the solid-like part, where the stress does not exceed the yield stress, was modeled with very large viscosity, the implicit velocity calculation was introduced so as to avoid the restriction of the time step width with respect to the diffusion number. As a result, the present model could express the stopping and solid-like behaviors, which are characteristics of Bingham fluids. The proposed method was verified and validated, and its capability was demonstrated through calculations of the two-dimensional Poiseuille flow of a Bingham plastic fluid and the three-dimensional dam-break flow of a Bingham pseudoplastic fluid by comparing those computed results to theory and experiment.

Keywords: Non-Newtonian fluid, Bingham fluid, Smoothed particle hydrodynamics, Moving particle semi-implicit, Physical consistency

1. Introduction

Particle methods, which are Lagrangian mesh-free approaches suitable for handling large deformations of free-surface flows, have attracted much interest in calculating complex flows with interfaces and multiple phases in various engineering fields. Representative methods are the Smoothed Particle Hydrodynamics (SPH) method developed by Lucy (1977), Gingold and Monaghan (1977), and the Moving Particle Semi-implicit (MPS) method developed by Koshizuka and Oka (1996). In the past two decades, owing to significant advancements in stability and accuracy, boundary treatments, physical models, acceleration techniques, and computational environment, the SPH and MPS methods have been applied to a variety of applications in ocean engineering, coastal engineering, naval engineering, civil engineering, nuclear engineering, and mechanical engineering (Violeau and Issa, 2007; Koshizuka, 2011; Gotoh and Khayyer, 2016; Violeau and Rogers, 2016; Shadloo et al., 2016; Wang et al., 2016; Koshizuka et al., 2018; Ye et al., 2019; Liu and Zhang, 2019; Lind et al., 2020; Li et al., 2020; Luo et al., 2021; Xie et al., 2022).

Bingham fluid calculation is a significant, active research topic in particle methods. Bingham fluids are encountered in a wide variety of applications, both environmental (e.g., mud, snow, ice, and blood) and industrial (e.g., lubricating grease, fresh concrete, suspensions, polymers, and paints). A Bingham fluid, such as the Bingham plastic fluid and the Bingham pseudoplastic fluid, is a non-Newtonian fluid with a distinctive yield stress and behaves as a solid below the

Paper No.23-00373
[DOI: 10.1299/jfst.2023jfst0035]

yield stress but flows as a highly viscous fluid above that. The non-Newtonian behavior arises because of a microscopic heterogeneous feature in the fluids, i.e., Bingham fluids contain dispersed phases such as thickener in lubricating greases (Lugt, 2013) and aggregate in fresh concrete (Xu and Li, 2021). The dispersed phases interact and have a microstructure that requires a certain amount of stress to break up. Once the microstructure is broken, the dispersed phase moves under viscous forces within the fluid (main composition). If the stress is removed, the dispersed phases reform the microstructure again.

In simulating Bingham fluids, there are two modeling approaches: (1) the continuum approach and (2) the microstructure approach (Ye et al., 2019; Rossi et al., 2022). In the continuum approach, a Bingham fluid is regarded as a homogeneous fluid without microstructure, and its non-Newtonian behavior is modeled by the constitutive equation that describes the relationship between the shear stress and the strain rate. Thus, the solid- and fluid-like behaviors of a Bingham fluid can be expressed by the change in viscosity, i.e., the fluid does not deform due to higher viscosity at a lower strain rate (resembling a solid), while the fluid flows due to moderate viscosity at a higher strain rate. Since the continuum approach is easy to implement into existing solvers and its computational cost is low, the SPH and MPS methods have been applied with the continuum approach to a wide variety of problems: Couette flows (Zhou et al., 2010), Taylor-Couette flows (Xu and Li, 2021), Poiseuille flows (Ren et al., 2012; Ikari et al., 2012; Xenakis et al., 2015; Ren et al., 2016; Tao et al., 2017; Morikawa et al., 2019), flows around a cylinder (Rossi et al., 2022), dam-break flows (Xenakis et al., 2015; Morikawa et al., 2019; Shao and Lo, 2003; Xu and Jin, 2016; Xie and Jin, 2016; Negishi et al., 2019; Abdolahzadeh et al., 2019), column-collapse flows (Xu and Jin, 2016; Minatti and Paris, 2015), L-box flows (Cao and Li, 2017; Xu et al., 2021), granular flow down an inclined plane (Minatti and Paris, 2015), impacting droplet (Xu et al., 2013), injection molding (Xu et al., 2013), jet buckling (Ren et al., 2016; Morikawa et al., 2019; Xu et al., 2013; de Souza Andrade et al., 2015), filling process in circular molds (Ren et al., 2012; Xenakis et al., 2015), filling process in a ring-shaped channel (Ren et al., 2012), two-dimensional flows in a two-dimensional cylinder and vane rheometers (Zhu et al., 2010), mixing process in mixers (Abdolahzadeh et al., 2019), splashing phenomena (Tao et al., 2017), landslide-induced tsunami (Ikari et al., 2012), and snow avalanches (Saito et al., 2012). In the microstructure approach, a Bingham fluid is assumed to be a multi-phase fluid consisting of continuous and dispersed phases, in which interactions and microstructures of the dispersed phases are directly considered. The SPH and MPS methods with this approach have been used to simulate fresh concrete flows, such as the slump flow test (Xu and Li, 2021; Deeb et al., 2014a), the L-box test (Xu and Li, 2021; Deeb et al., 2014b), and pipe flows (Xu et al., 2022). However, the microstructure approach employed in those studies has been limited to the cases where the dispersed phase has a relatively large structure, such as coarse aggregates or fibers in fresh concrete, and it is still too expensive to resolve microscale materials such as thickener (large molecules) in lubricating greases and colloids in suspensions. Therefore, the continuum approach still prevails in Bingham fluid calculations.

Particle-based simulations of highly viscous fluids, such as the solid state of Bingham fluids, are still challenging because of two issues: (1) numerical stability against high viscosity and (2) linear and angular momentum conservation (Kondo et al., 2022). When the viscosity term is calculated explicitly for high-viscous flows, where the viscous forces are dominant, the time step size needs to be set small enough to meet the stability condition of the viscosity term (Duan and Chen, 2013), which results in unfavorably high computational costs. To overcome this issue, the implicit velocity calculation was adopted to cope with the high viscosity in some of the previous studies with the SPH (Morikawa et al., 2019; Takahashi et al., 2015; Zago et al., 2018; Weiler et al., 2018) and with the MPS method (Xu and Li, 2021; Negishi et al., 2019; Xu et al., 2021; Xu et al., 2022). In addition to the high viscosity treatment, the linear and angular momentum conservation is also important for calculating the solid-like behavior in Bingham fluid. However, the conventional difference-based Laplacian models for the viscosity term, often adopted in the SPH and MPS methods, result in unphysical suppression of the rotational motion due to the torque against rotation (Kondo et al., 2022). To overcome this problem, the SPH method incorporates several improvements, such as the gradient correction (Ren et al., 2016; Abdolahzadeh et al., 2019; Frissane et al., 2019; Xu and Deng, 2016) and the pairwise-damping viscosity model (Ren et al., 2012; Ren et al., 2016; Minatti and Paris, 2015; Weiler et al., 2018; Pan et al., 2013; Russell et al., 2018; Monaghan, 2019).

Currently, a very limited number of particle methods that employ implicit velocity calculation and simultaneously conserve the linear and angular momentum are found. One is the SPH model proposed by Weiler et al. (2018), and the other is the Moving Particle Hydrodynamics (MPH) method (Kondo et al., 2022). Both methods adopted the pairwise-damping model for angular momentum conservation within the implicit calculation. The major difference between the

[DOI: 10.1299/jfst.2023jfst0035]

two is physical consistency. When the discretized system satisfies the fundamental laws of physics, i.e., mass conservation, linear and angular momentum conservation, and the second law of thermodynamics, the method is termed physically consistent. Since the MPH method is physically consistent, other fundamental laws of physics are also satisfied as well as the linear and angular momentum conservation. In the previous MPH studies (Kondo and Matsumoto, 2021; Kondo, 2021; Negishi et al., 2023), this feature was revealed important for the stability of the discrete particle system. The MPH method does not need empirical stabilizing techniques, such as the artificial repulsive force (Koshizuka et al., 1998; Monaghan, 2000), zero-pressure limiter (Koshizuka et al., 1998), collision (Lee et al., 2011), and particle shifting (Xu et al., 2009; Khayyer et al., 2017), which were often introduced in the conventional particle method, i.e., the SPH and MPS methods. Therefore, it seems better to adopt the physically consistent particle method, i.e., the MPH method, in terms of robustness and soundness of the calculation. The verification and validation were conducted in the previous works on the MPH method with various numerical examples (Kondo et al., 2022; Kondo and Matsumoto, 2021; Kondo, 2021; Negishi et al., 2023).

In this study, a Bingham fluid simulation model was constructed and validated based on the physically consistent particle method, i.e., the MPH method. In the MPH method, there are two versions: one is the incompressible version termed “MPH-I” (Kondo, 2021), in which the practically incompressible condition is considered, and the other is the weakly compressible version termed “MPH-WC” (Kondo and Matsumoto, 2021), in which the weakly compressible assumption is considered. The current study employed the MPH-WC method with the implicit velocity calculation because of its high computational efficiency. Adopting the continuum approach, the viscosity was varied based on the constitutive models for the Bingham fluids. The two-dimensional Poiseuille flow of a Bingham plastic fluid and the three-dimensional dam-break flow of a Bingham pseudoplastic fluid were calculated to verify and validate the proposed numerical method. This paper compares the computed results to theory and experiment.

2. Numerical method

2.1 Discretization of governing equation

This study employs MPH for weakly compressible flows method (MPH-WC) (Kondo et al., 2022; Kondo and Matsumoto, 2021). The governing equations are the Navier-Stokes equation

$$\rho_0 \frac{D\mathbf{u}}{Dt} = -\nabla\Psi + \nabla\cdot\left(\mu\nabla\mathbf{u}\right) + \rho_0\mathbf{g} \tag{1}$$

and the pressure equation

$$\Psi = -\lambda\nabla\cdot\mathbf{u} + \kappa\frac{\rho-\rho_0}{\rho_0}, \tag{2}$$

where ρ_0, ρ, $\mathbf{u}$, t, Ψ, μ, $\mathbf{g}$, λ, and κ are the reference density, density, velocity, time, pressure, shear viscosity, gravity, bulk viscosity, and bulk modulus, respectively. In the MPH method, specifying large values for bulk viscosity λ and bulk modulus κ can express practical incompressibility in calculations.

The MPH method (Kondo et al., 2022; Kondo and Matsumoto, 2021; Kondo, 2021; Negishi et al., 2023) uses the discretized governing equations derived by particle interaction models in a similar way to the SPH (Lucy, 1977; Gingold and Monaghan, 1977) and MPS methods (Koshizuka and Oka, 1996) based on effective radius h and the weight function. The weight function is expressed as

[DOI: 10.1299/jfst.2023jfst0035]

$$
\begin{aligned}
w_{ij} &= w\ (|\mathbf{r}_{ij}|) \\
w\ (r) &= \begin{cases} \dfrac{1}{S_f} f\left(r\right) & (r \le h\ ) \\ 0 & (r > h\ ) \end{cases} \\
f\left(r\right) &= \frac{1}{h^{\,d}}\left(1-\frac{r}{h}\right)^2 \\
S_f &= -\frac{1}{d}\sum_{i\neq j}\left|\mathbf{r}_{ij}\right|\frac{\partial f\left(\left|\mathbf{r}_{ij}\right|\right)}{\partial r},
\end{aligned}
\tag{3}
$$

where $\mathbf{r}_{ij} = \mathbf{r}_j - \mathbf{r}_i$ is the relative position vector from particle i to j, r is the absolute value of $\mathbf{r}_{ij}$, h is the effective radius, d is the space dimension, and S_f is a normalized parameter, which is calculated using an equally-spaced particle distribution before starting the calculation. The first term on the right-hand side of Eq. (1) is the negative pressure gradient, which is discretized as

$$
\left\langle \nabla\Psi \right\rangle_i = -\sum_{j\neq i}(\Psi_j + \Psi_i)\mathbf{e}_{ij} w_{ij}',
\tag{4}
$$

the second term is the shear viscosity, which is discretized using the pairwise-damping model (Kondo et al., 2022) as

$$
\left\langle \nabla\cdot\left(\mu\nabla\mathbf{u}\right)\right\rangle_i = -2(d+2)\sum_{j\neq i}\left(\frac{2\mu_i\mu_j}{\mu_i+\mu_j}\frac{\mathbf{u}_{ij}}{\left|\mathbf{r}_{ij}\right|}\cdot\mathbf{e}_{ij}\right)\mathbf{e}_{ij} w_{ij}'.
\tag{5}
$$

Here, the harmonic mean interparticle viscosity (Duan et al., 2015) is adopted to model the interaction between particles with different shear viscosities. The first term on the right-hand side of Eq. (2) is the bulk viscosity, which is discretized as

$$
\left\langle \lambda\nabla\cdot\mathbf{u}\right\rangle_i = -\lambda\sum_{j\neq i}\left(\mathbf{u}_{ij}\cdot\mathbf{e}_{ij}\right)w_{ij}'.
\tag{6}
$$

In Eqs. (4), (5), and (6), the symbol $<>_i$ indicates the application of the particle interaction models of the MPH method around particle i; the vector $\mathbf{e}_{ij} = \mathbf{r}_{ij}/\left|\mathbf{r}_{ij}\right|$ is the unit vector from particle i to j; the vector $\mathbf{u}_{ij} = \mathbf{u}_j - \mathbf{u}_i$ is the relative velocity from particle i to j; w_{ij}' is the space derivative of the weight function w_{ij} expressed as

$$
\begin{aligned}
w_{ij}' &= w'(|\mathbf{r}_{ij}|) \\
w'(r) &= \frac{\partial w\ (r)}{\partial r},
\end{aligned}
\tag{7}
$$

which has a negative value. The second term on the right-hand side of Eq. (2), the bulk modulus term, is discretized using the continuity equation (Kondo et al., 2022)

$$
\kappa\frac{\rho-\rho_0}{\rho_0} \approx \kappa(n_i - n_0),
\tag{8}
$$

where n_i is the particle number density defined as

[DOI: 10.1299/jfst.2023jfst0035]

$$n_i = \sum_{j \neq i} w_{ij}, \tag{9}$$

and n_0 is a base value evaluated using an equally-spaced particle distribution before computation. As a result, the governing equations of Eqs. (1) and (2) are discretized as

$$M \frac{d\mathbf{u}_i}{dt} = \sum_{j \neq i} (\Psi_j + \Psi_i) \mathbf{e}_{ij} w_{ij}' \Delta V - 2(d+2) \sum_{j \neq i} \left(\frac{2\mu_i \mu_j}{\mu_i + \mu_j} \frac{\mathbf{u}_{ij}}{|\mathbf{r}_{ij}|} \cdot \mathbf{e}_{ij} \right) \mathbf{e}_{ij} w_{ij}' \Delta V + M\mathbf{g} \tag{10}$$

and

$$\Psi_i = \lambda \sum_{j \neq i} \left(\mathbf{u}_{ij} \cdot \mathbf{e}_{ij} \right) w_{ij}' + \kappa (n_i - n_0), \tag{11}$$

respectively, where ΔV is the volume of a single particle region, which is a constant given by the initial particle spacing l_0 as $\Delta V = l_0^d$, and M is the mass of a single particle ($=\rho_0 \Delta V$). To avoid the tensile instability (Monaghan, 2000), the second term on the right-hand side of Eq. (11) is ignored when $n_i - n_0 < 0$. In addition, the solid wall is modeled by wall particles with specific positions and velocities.

In the MPH method, the discretized equations (10) and (11) are fitted into the analytical mechanical framework for systems with dissipation (Kondo et al., 2022), which ensures a monotonic decrease of the mechanical energy following the second law of thermodynamics. This key feature is especially useful for dynamically stable calculations without artificial relaxation parameters or numerical techniques for stabilization. Furthermore, linear and angular momentum conservation can also be satisfied by incorporating the symmetric pressure gradient model of Eq. (4) and the pairwise-damping viscosity model of Eq. (5).

2.2 Constitutive model for Bingham fluid

This study considers Bingham fluid, in specific Bingham plastic and Bingham pseudoplastic fluids, as working fluid in its simulations. Bingham fluid is a non-Newtonian fluid with solid- and fluid-like behaviors, which has a certain yield stress and behaves like a solid below the stress but flows as highly viscous fluid above it. Here, Bingham fluid is modeled by the continuum approach (Ye et al., 2019; Rossi et al., 2022), in which it is regarded as a homogeneous fluid; its non-Newtonian behaviors are expressed by the strain-rate dependence of shear viscosity based on the constitutive equation describing the stress-strain relation, i.e., solid-like behavior is modeled by high viscosity at a lower strain rate, and fluid-like behavior is by moderate viscosity at a higher strain rate.

In this study, we applied two types of Bingham models, i.e., the Bingham plastic and pseudoplastic models. Specifically, the shear viscosity-strain rate relation for Bingham plastic fluid is given by

$$\mu(\dot{\gamma}) = \mu_p + \frac{\tau_Y}{\dot{\gamma}}, \tag{12}$$

and that for Bingham pseudoplastic fluid is given by

$$\mu(\dot{\gamma}) = K\dot{\gamma}^{n-1} + \frac{\tau_Y}{\dot{\gamma}}. \tag{13}$$

Here, τ_Y is the yield stress; μ_p is the plastic viscosity (which is the limiting viscosity at a high strain rate); $\dot{\gamma}$ is the equivalent strain rate; K is the consistency index; n is the flow index, representing the shear-thinning behavior if $n < 1.0$. Using Eqs. (12) and (13) directly is not useful in practical calculations because the viscosity of Eqs. (12) and (13) gives an infinite value when $\dot{\gamma} \to 0$, leading to a numerical divergence. To avoid this singularity, the Papanastasiou regularization is used in calculations (Papanastasiou, 1987). The Bingham plastic model with the Papanastasiou regularization based on Eq. (12), i.e., the regularized Bingham model, is expressed as

[DOI: 10.1299/jfst.2023jfst0035]

$$\mu(\dot{\gamma}) = \mu_p + \frac{\tau_Y}{\dot{\gamma}}\left(1 - e^{-m|\dot{\gamma}|}\right), \tag{14}$$

and the Bingham pseudoplastic model with the Papanastasiou regularization based on Eq. (13), i.e., the Herschel-Bulkley-Papanastasiou (HBP) model (Mitsoulis, 2008), is given as

$$\mu(\dot{\gamma}) = K\dot{\gamma}^{n-1} + \frac{\tau_Y}{\dot{\gamma}}\left(1 - e^{-m|\dot{\gamma}|}\right). \tag{15}$$

Here, m is the Papanastasiou regularization parameter, which controls the stress exponential growth, i.e., the transition between solid and fluid regimes. The larger the m is, the sharper the transition is.

The equivalent strain rate $\dot{\gamma}$ is the second principal invariant of the strain rate tensor $\mathbf{S}$, which is defined as

$$\begin{aligned} \dot{\gamma} &= \sqrt{2\mathbf{S}:\mathbf{S}} \\ \mathbf{S} &= \frac{1}{2}\left((\nabla \otimes \mathbf{u}) + (\nabla \otimes \mathbf{u})^T\right). \end{aligned} \tag{16}$$

The velocity gradient tensor $\nabla \otimes \mathbf{u}$ in Eq. (16) for particle i is evaluated by the following expression:

$$\langle \nabla \otimes \mathbf{u} \rangle_i = -\sum_{j \neq i} \left(\mathbf{u}_{ij} \otimes \mathbf{e}_{ij}\right) w'_{ij}. \tag{17}$$

2.3 Time integration

The time integration algorithm of the MPH-WC method with the implicit velocity calculation (Kondo et al., 2022), along with the Bingham fluid modeling, is shown in Fig. 1. The upper index k in the equations of the figure indicates the time step.

After the explicit calculation of the pressure

$$\Psi_i^k = \lambda \sum_{j \neq i} \left(\mathbf{u}_{ij}^k \cdot \mathbf{e}_{ij}\right) w_{ij}' + \kappa(n_i^k - n_0). \tag{18}$$

and the shear viscosity

$$\begin{aligned} \mu_i^k &= \mu\left(\dot{\gamma}_i^k\right) \\ \dot{\gamma}_i^k &= \sqrt{2\mathbf{S}_i^k : \mathbf{S}_i^k} \\ \mathbf{S}_i^k &= \frac{1}{2}\left(\left(-\sum_{j \neq i}\left(\mathbf{u}_{ij}^k \otimes \mathbf{e}_{ij}\right) w'_{ij}\right) + \left(-\sum_{j \neq i}\left(\mathbf{u}_{ij}^k \otimes \mathbf{e}_{ij}\right) w'_{ij}\right)^T\right), \end{aligned} \tag{19}$$

the velocity is calculated implicitly as

$$M\frac{\mathbf{u}_i^{k+1} - \mathbf{u}_i^k}{\Delta t} = \sum_{j \neq i}\left(\Psi_j^k + \Psi_i^k\right)\mathbf{e}_{ij} w_{ij}' \Delta V - 2(d+2)\sum_{j \neq i}\left(\frac{2\mu_i^k \mu_j^k}{\mu_i^k + \mu_j^k}\frac{\mathbf{u}_{ij}^{k+1}}{|\mathbf{r}_{ij}|} \cdot \mathbf{e}_{ij}\right)\mathbf{e}_{ij} w_{ij}' \Delta V + M\mathbf{g}. \tag{20}$$

Then, the position is updated as

$$\mathbf{r}_i^{k+1} = \mathbf{r}_i^k + \mathbf{u}_i^{k+1}\Delta t \tag{21}$$

[DOI: 10.1299/jfst.2023jfst0035]

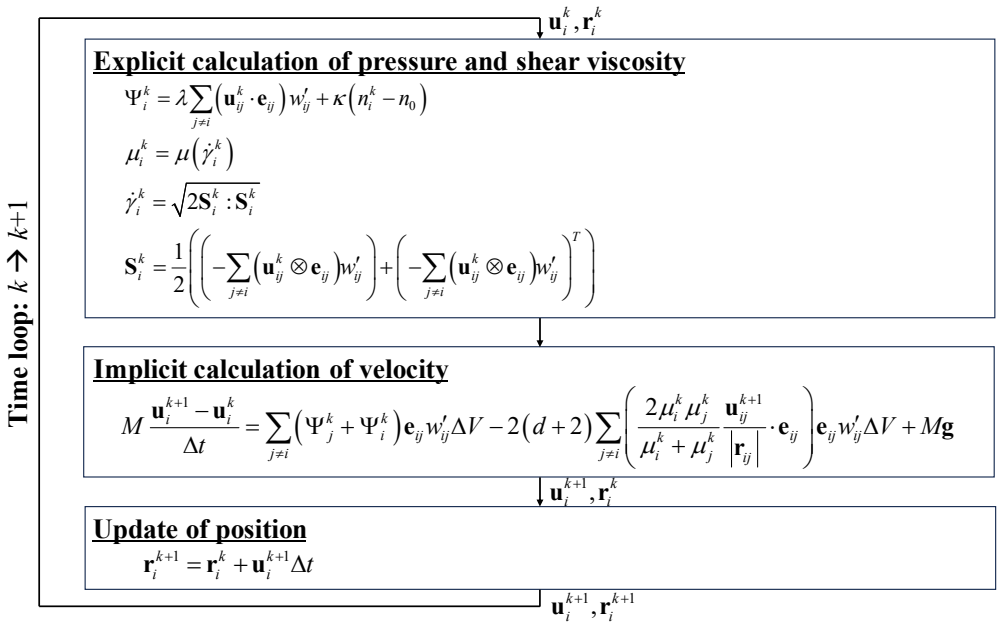

Fig. 1 Time integration algorithm of the MPH-WC method with the implicit velocity calculation along with the Bingham fluid modeling.

at the end of the time step. Here, Δt is the time step size.

Since the matrix equation given by Eq. (20) is symmetric positive definite, the conjugated gradient (CG) solver is employed. For its implementation, the linear systems (Lis) library (Nishida, 2010; Lis: Library of Iterative Solvers for Linear Systems (online)) was utilized in this study.

In this approach, it should be noted that the shear viscosity term, i.e., the second term on the right-hand side of Eq. (20), is implicitly calculated, whereas the bulk viscosity term, i.e., the first term on the right-hand side of Eq. (18), is explicitly calculated. This treatment is valid when a large pressure load is not expected such as in the considered test cases shown in Section 3 of this study. In our past study (Kondo et al., 2022), the validity of this approach was demonstrated in test cases of a rotating circular pipe, high-viscous Taylor-Couette flow, and offset collision of a high-viscous object.

When using a fully explicit time integration scheme in the particle methods including the MPH-WC method, the time step size Δt needs to be specified considering the stability conditions based on the Courant number C_{CFL} and the diffusion number C_{DIF} expressed as

$$C_{CFL} = \frac{u_{max} \Delta t}{l_0} < C_{CFL,max} \tag{22}$$

and

$$C_{DIF} = \frac{\mu_{max} \Delta t}{\rho_0 l_0^2} < C_{DIF,max}, \tag{23}$$

where l_0 is the initial particle spacing, u_{max} is the maximum flow velocity, μ_{max} is the maximum viscosity, and $C_{CFL,max}$ and $C_{DIF,max}$ are the superior thresholds of C_{CFL} and C_{DIF} for numerical stability. Eq. (22) is the Courant stability condition and Eq. (23) is the stability condition of the viscosity term. $C_{CFL,max}$ and $C_{DIF,max}$ are empirically set to values between 0.1 and 0.5, respectively (Duan and Chen, 2013; Koshizuka et al., 2018; Zago et al., 2018). With the implicit time integration of the shear viscosity term, $C_{DIF,max}$ can be a higher value than the conventional threshold in the current method. In the current study, only the Courtant stability condition Eq. (22) with $C_{CFL,max} = 0.1$ was considered as the stability condition.

[DOI: 10.1299/jfst.2023jfst0035]

3. Calculation examples

3.1 Two-dimensional Poiseuille flow

To verify the proposed approach for steady-state shear phenomena of a Bingham fluid, a two-dimensional Poiseuille flow was calculated. This test case is from Ikari et al. (2012), in which the velocity profile of the Bingham plastic fluid was discussed and compared with the theoretical result. The computational model is illustrated in Fig. 2, and the calculation conditions are shown in Table 1. The working fluid is the Bingham plastic fluid, which is modeled by Eq. (14). The shear stress ($\tau = \mu(\dot{\gamma})|\dot{\gamma}|$) and shear viscosity are displayed in Fig. 3. In the computational domain, the two no-slip walls with a length of L = 5.0 m are separated by a distance of $2H$ = 1.0 m. The no-slip walls were modeled by five layers of wall particles by specifying a zero velocity. The gravitational acceleration $\mathbf{g} = (g_x, g_y) = (0.1\ \mathrm{m/s^2}, 0.0\ \mathrm{m/s^2})$ and the periodic boundary conditions were imposed in the x direction. In calculations, the three different particle spacings of l_0 = 50 mm, 25 mm, and 12.5 mm were applied to evaluate the influence of the particle resolution. Their diffusion number C_{DIF} was 3.2, 6.4, and 12.8, respectively. Furthermore, the four effective radii of $h = 2.1l_0$, $3.1l_0$, $4.1l_0$, and $5.1l_0$ were also investigated to check the influence of the effective radius h.

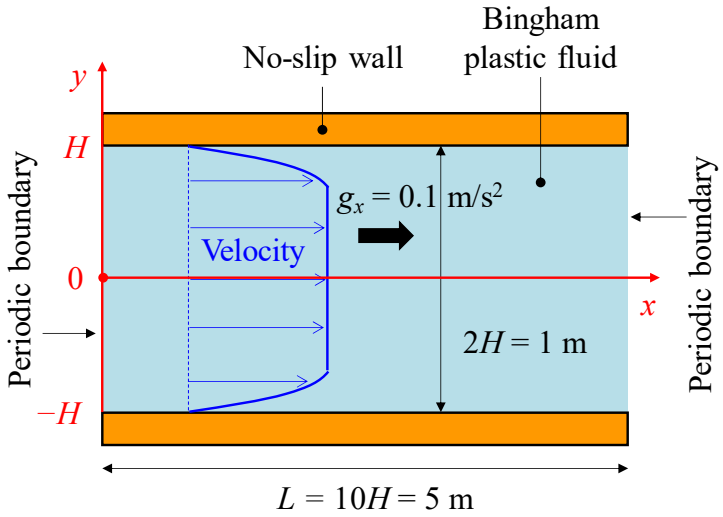

Fig. 2 Schematic of two-dimensional Poiseuille flow.

Table 1 Calculation conditions for two-dimensional Poiseuille flow.

Parameters	Coarse case	Base case	Fine case
Fluid reference density ρ_0 (kg/m^3)	1000		
Plastic viscosity η_p (Pa-s)	10.0		
Yield stress τ_Y (Pa)	20.0		
Regularization parameter m (-)	100.0		
Gravitational acceleration g_x (m/s^2)	0.1		
Initial particle spacing l_0 (m)	50.0 x 10^{-3}	25.0 x 10^{-3}	12.5 x 10^{-3}
Effective radius h (m)	$2.1l_0$, $3.1l_0$, $4.1l_0$, $5.1l_0$		
Bulk viscosity λ (Pa-s)	6.0 x 10^2	3.0 x 10^2	1.5 x 10^2
Bulk modulus κ (Pa)	1.5 x 10^5		
Time step width Δt (s)	4.0 x 10^{-3}	2.0 x 10^{-3}	1.0 x 10^{-3}
Number of particles N	2958	9898	35867

[DOI: 10.1299/jfst.2023jfst0035]

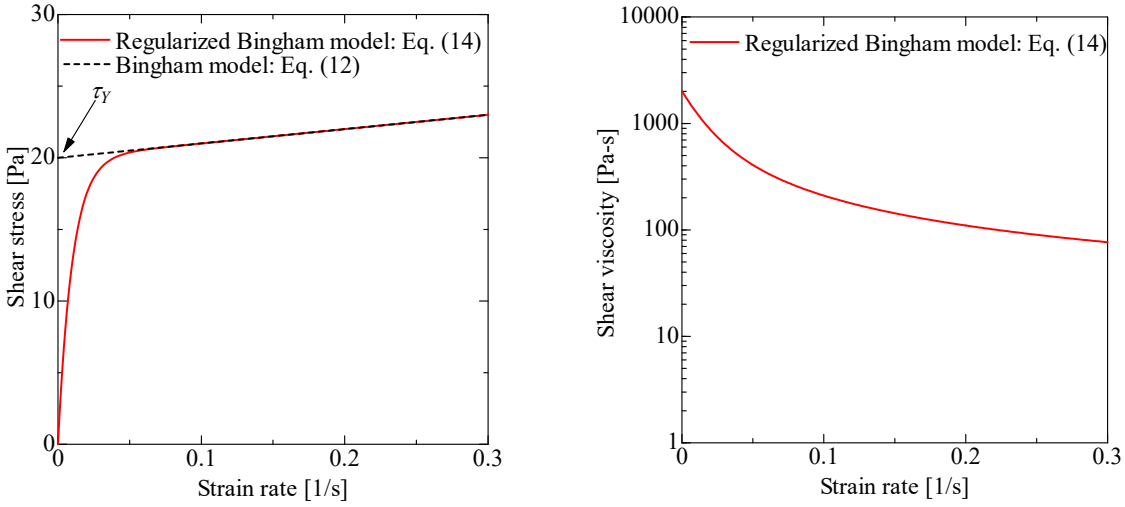

(a) Shear stress (b) Shear viscosity

Fig. 3 Shear stress and viscosity of Bingham plastic fluid.

Figure 4 compares the velocity profile between the theory and calculation. Here, the theoretical velocity profile of a Bingham plastic fluid in a two-dimensional channel is given (Ikari et al., 2012) by

$$u(y)=\begin{cases}\dfrac{\rho_0 g_x}{2\mu_p}\left(H-y_0\right)^2 & \left(0\le|y|\le y_0\right)\\[2ex] \dfrac{\rho_0 g_x}{2\mu_p}\left(H^2-|y|^2\right)-\dfrac{\tau_Y}{\mu_p}\left(H-|y|\right) & \left(y_0\le|y|\le H\right)\end{cases} \tag{24}$$

$$y_0=\frac{\tau_Y}{\rho_0 g_x}.$$

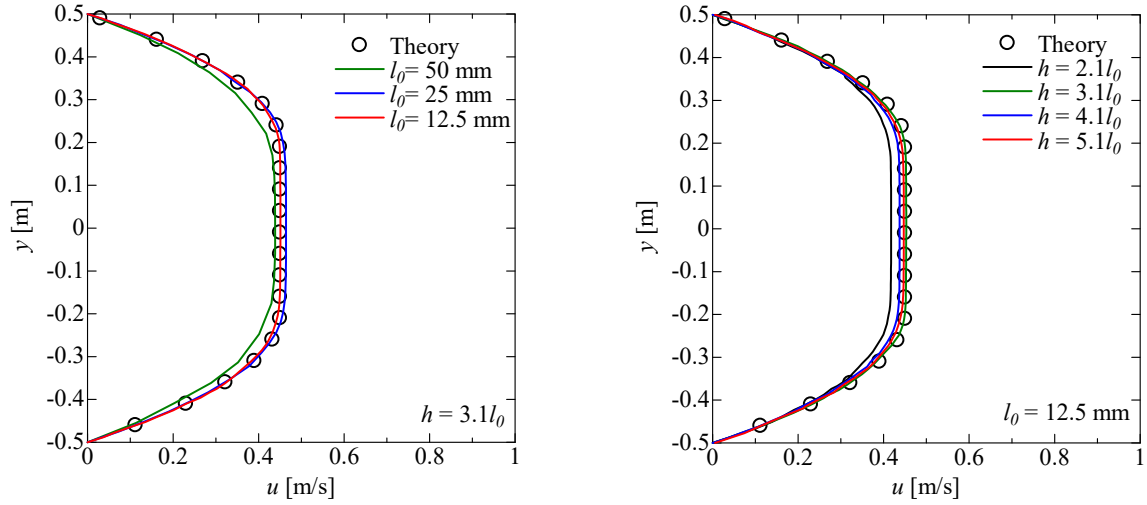

(a) Influence of particle spacing (h=3.1l_0) (b) Influence of effective radius (l_0=12.5 mm)

Fig. 4 Comparison of velocity profile between theory and calculation.

[DOI: 10.1299/jfst.2023jfst0035]

Figure 4 (a) shows the influence of particle spacing with the effective radius of $h = 3.1l_0$. Although $l_0 = 50$ mm underpredicted the velocity profile slightly, the spacings of $l_0 = 25$ mm and 12.5 mm showed reasonable agreement with the theory. The influence of the effective radius with the particle spacing of $l_0 = 12.5$ mm is shown in Fig. 4 (b). Although the effective radius of $h = 2.1l_0$ underpredicted the velocity profile, the effective radii of $3.1l_0$, $4.1l_0$, and $5.1l_0$ showed reasonable agreement with the theory. Between the three effective radii, $h = 3.1l_0$ showed the best agreement with the theory, indicating the optimum effective radius. The effective radius remains as an arbitrary parameter for the particle interaction models, Eqs. (4), (5), and (6), even in the current method like in the MPS method (Koshizuka et al., 2018). A too-small effective radius reduces the space accuracy of approximations, whereas a too-large effective radius gives diffusive solutions of a local region. Furthermore, a large effective radius increases the number of neighboring particles, i.e., the computational cost, which cannot be acceptable for practical use. Therefore, an optimum effective radius should be selected, considering the balance between accuracy and computational cost. Ikari et al. (2012) obtained a similar result and conclusion. As a result, it was confirmed that the proposed approach can be applied to the shear phenomena of a Bingham fluid with confidence.

3.2 Three-dimensional dam-break flow

The dam-break flow of a Bingham pseudoplastic fluid was simulated in three-dimensions to validate the proposed approach for a dynamic problem involving solid- and fluid-like behaviors. Specifically, the dam-break experiment using lubricant grease conducted in the past study (Negishi et al., 2019) was calculated.

A cross-sectional view of the three-dimensional computational model on the symmetry plane in the initial state is displayed in Fig. 5, and the calculation conditions are shown in Table 2. The working fluid, a Bingham pseudoplastic fluid, is modeled by Eq. (15). The shear stress ($\tau = \mu(\dot{\gamma})|\dot{\gamma}|$) and viscosity are displayed in Fig. 6. The internal space of the tank was 570 mm x 210 mm x 100 mm. Initially, the fluid was placed behind a fixed partition with a movable gate, creating a column measuring 100 mm x 140 mm x 100 mm in a vertical reservoir. The thickness of the fixed partition and movable gate is 15 mm. All the walls, which include the tank wall, the fixed partition, and the movable gate, were modeled by the wall particles, and five layers of the wall particles were given in the thickness direction for the tank wall. The no-slip condition was imposed for all the stationary walls by setting a zero velocity, and an upward velocity of 0.6 m/s was specified for the movable gate until $t = 0.15$ s. The gravitational acceleration $\mathbf{g} = (g_x, g_y, g_z) = (0.0\ \text{m/s}^2,\ -9.8\ \text{m/s}^2,\ 0.0\ \text{m/s}^2)$ was imposed. In calculations, the four different particle spacings of $l_0 = 5.0$ mm, 3.0 mm, 1.5 mm, and 1.0 mm were applied to evaluate the influence of the particle resolution. Their diffusion number C_{DIF} was 87.6, 147.9, 297.6, and 446.7, respectively. The effective radius h was set to $3.1l_0$.

Figure 7 (a) shows a set of snapshots of the dam-break flow obtained by the experiment (Negishi et al., 2019). It should be noted that the experimental results in Fig. 7 (a) are side views because of restricted optical access. After the

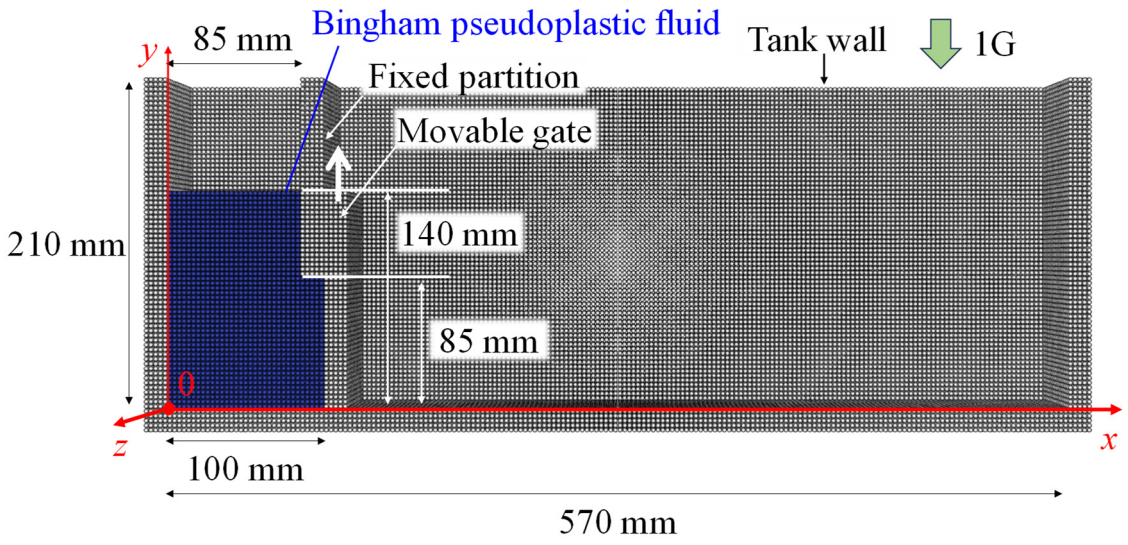

Fig. 5 Cross-sectional view of computational model of three-dimensional dam-break flow (The particle resolution is $l_0 = 3$ mm).

[DOI: 10.1299/jfst.2023jfst0035]

gate is removed with an upward velocity of 0.6 m/s at t = 0.0 s, the column collapses and spreads into the tank, creating a dam-break flow. The collapse continued as time passed t = 0.1 s, 0.2 s, and 0.3 s, and then it slowed down immediately after t = 0.5 s, showing a "boot-like" shape. Finally, the collapse stopped completely after t = 2.0 s.

Figure 7 (b) shows a set of snapshots of the dam-break flow calculated by the proposed method with the finest particle spacing of l_0 = 1.0 mm. Here, the computed results in Fig. 7 (b) are the cross-sectional views of the computational domain for visualization purposes. The computed results agreed with the experimental results regarding the free-surface shape. The velocity magnitude profile in Fig. 7(b) helps us understand the dam-break flow in detail. During the collapse, the flow velocity at the left bottom corner is almost zero because the fluid is subjected to the two boundary resistances from the side and bottom walls of the tank, whereas the fluid near the free surface and in the front of the flow moves very quickly. After the fluid rushed out of the reservoir, the fluid slowed down and almost stopped after t = 0.5 s. Finally, the maximum velocity magnitude reached less than 0.001 m/s at t = 2.0 s.

Table 2 Calculation conditions for three-dimensional dam-break flow.

Parameters	Coarse case	Base case	Fine case	Super-fine case
Fluid reference density ρ_0 (kg/m^3)	870			
Regularization parameter m (-)	200			
Consistency index K (-)	3.93			
Flow index n (-)	0.61			
Yield stress τ_Y (Pa)	57.0			
Regularization parameter m (-)	200.0			
Initial particle spacing l_0 (m)	5.0×10^{-3}	3.0×10^{-3}	1.5×10^{-3}	1.0×10^{-3}
Effective radius h (m)	1.55×10^{-2}	9.3×10^{-3}	4.65×10^{-3}	3.1×10^{-3}
Bulk viscosity λ (Pa-s)	125.0	75.0	37.5	25.0
Bulk modulus κ (Pa)	7.5×10^5			
Time step width Δt (s)	1.66×10^{-4}	1.0×10^{-4}	5.0×10^{-5}	3.33×10^{-5}
Number of particles N	92800	267744	1284108	3462000

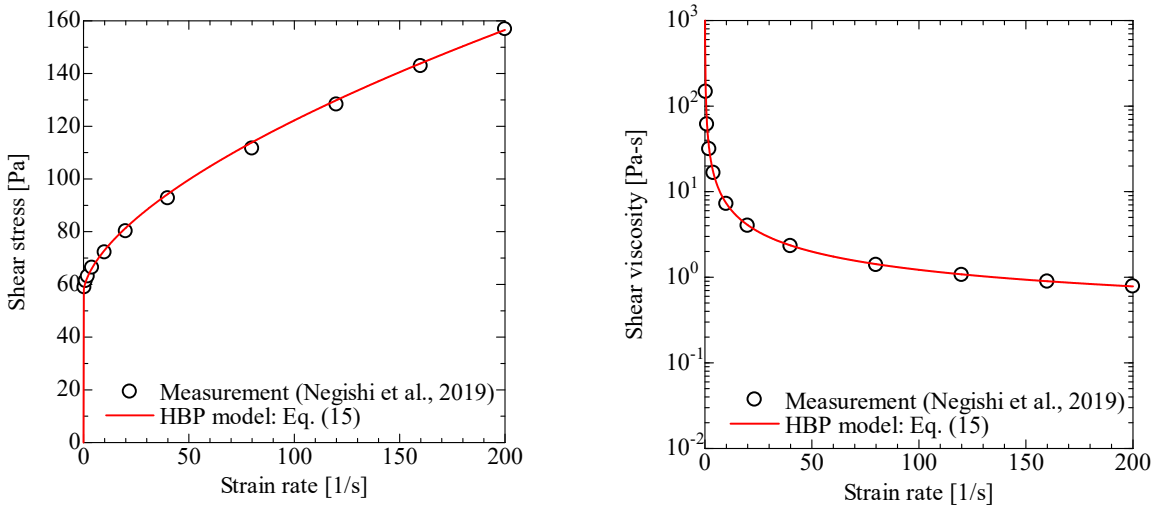

(a) Shear stress (b) Shear viscosity

Fig. 6 Shear stress and viscosity of Bingham pseudoplastic fluid.

[DOI: 10.1299/jfst.2023jfst0035]

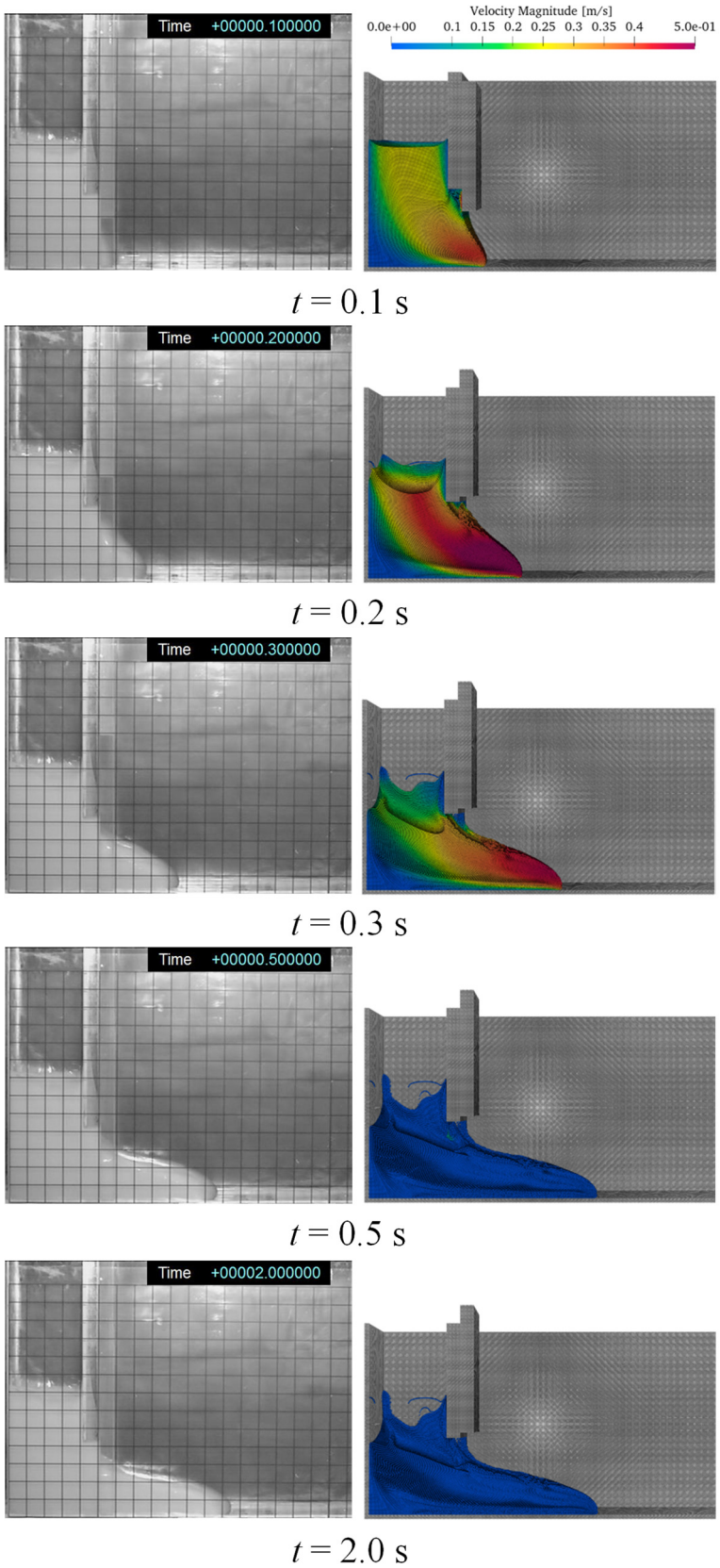

(a) Exp. (Negishi et al., 2019) (b) Calc. (velocity magnitude)

Fig. 7 Comparison of dam-break flow between experiment and calculation with particle resolution of l_0 = 1.0 mm. The velocity magnitude is also plotted in the calculated results. Please note that Fig. 7 (a) shows the side views, and Fig. 7 (b) shows the cross-sectional views.

[DOI: 10.1299/jfst.2023jfst0035]

Figures 8 (a) and (b) show the distributions of the equivalent strain rate and kinematic viscosity calculated with the finest particle spacing of $l_0 = 1.0$ mm, respectively. In Fig. 8 (a), a higher equivalent strain rate was observed in the region, in which the velocity gradient was high as shown in Fig. 7 (b), during the collapse until $t = 0.3$ s. After $t = 0.5$ s, overall, the equivalent strain rate significantly decreased because the collapse immediately slowed down and the velocity gradient in the collapse disappeared. Figure 8 (b) shows the kinematic viscosity distributions corresponding to the equivalent

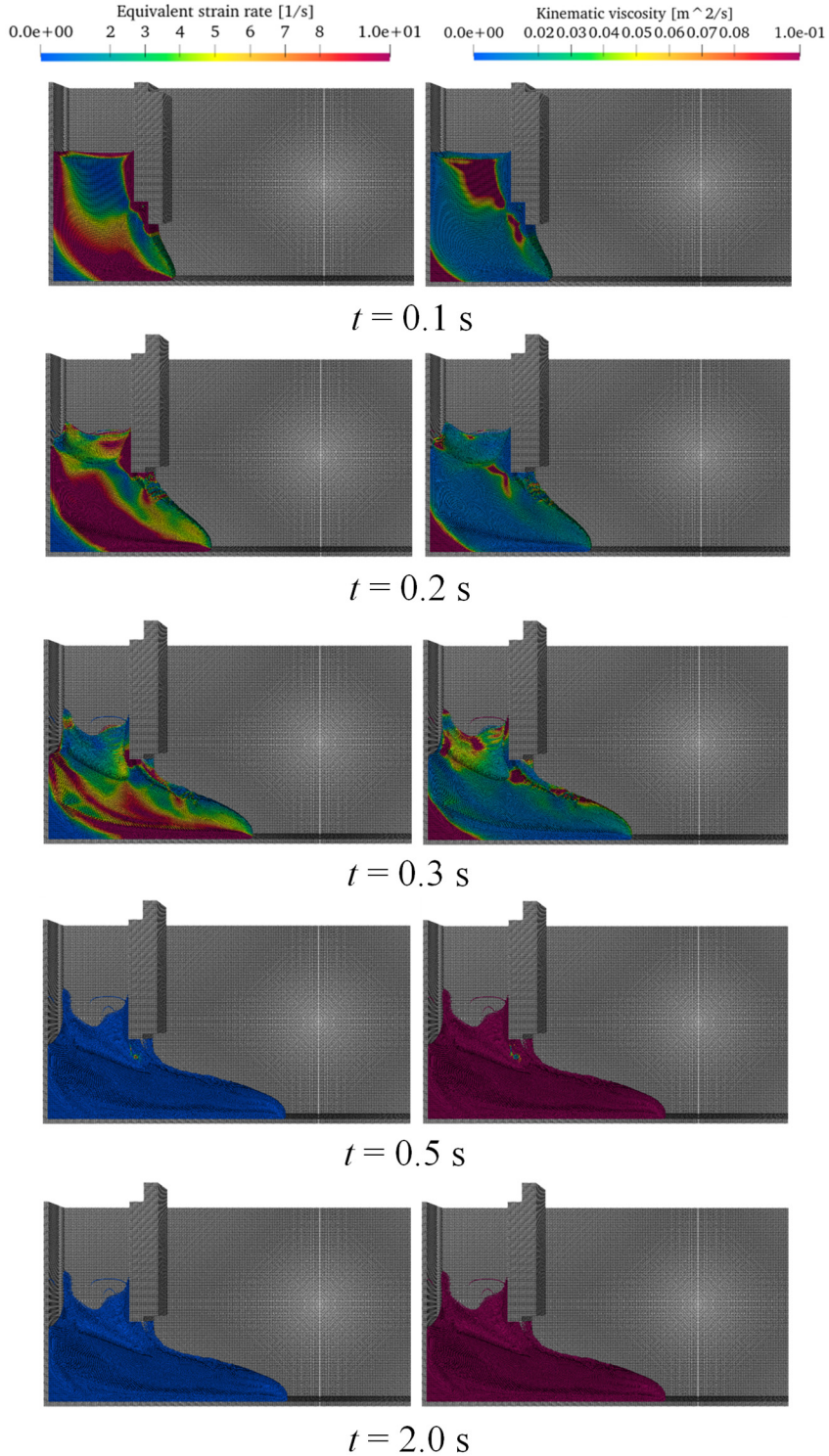

(a) Equivalent strain-rate (b) Kinematic viscosity

Fig. 8 Computed equivalent strain rate and kinematic viscosity distributions on the cross-section (The particle resolution of $l_0 = 1.0$ mm).

[DOI: 10.1299/jfst.2023jfst0035]

strain rate distributions in Fig. 8 (a). The higher the equivalent strain rate is, the lower the kinematic viscosity is. After the dam-break flow almost stopped at t = 0.5 s, the entire column had quite a high kinematic viscosity. This indicated that the proposed method could express the stopping and solid-like behaviors of the Bingham pseudoplastic fluid due to high viscosity.

A quantitative comparison of the front position of the dam-break flow between the experimental and computed results is shown in Fig. 9. Here, the computed results showed a reasonable qualitative agreement with the experimental data regardless of the particle spacing, showing the fluid phase with the immediate development of the front position until t = 0.5 s and the solid-like phase with the constant position, i.e., the stopping behavior, after t = 2.0 s. Quantitatively, a reasonable tendency toward convergence was observed in the computed results, showing a reasonable agreement with the experimental result using l_0 = 1 mm in the considered cases.

Comparing the experimental and calculated results in detail in Fig. 9, there seems to be some discrepancy around t = 0.5 s, corresponding to the shift of the moving phase to the stopping phase of the dam-break flow. The curves of the calculated results exhibit cliff edges, while the curve is smoother in the experiment. This discrepancy may be caused by the omission of small-scale phenomena like the slip layer or lubrication layer, which is a very thin layer in the vicinity of the wall and induces friction between the wall and fluid and a viscous force caused by local rotational motion of a fluid (Xu et al., 2021 and 2022). Xu et al. (2021) applied a macroscopic model, which is called the boundary slippage resistance model and locally evaluates additional wall shear stress, to a dam-break flow of fresh concrete and improved the history of the front position, smoothing the shift from the moving phase to the stopping phase. The improvement in this aspect is left to the future study.

As a result, it was confirmed that the proposed approach could be applied to the dynamic behavior of a Bingham pseudoplastic fluid involving the solid- and fluid-like behaviors even with a high diffusion number C_{DIF} on the order of 10^2 in the considered conditions.

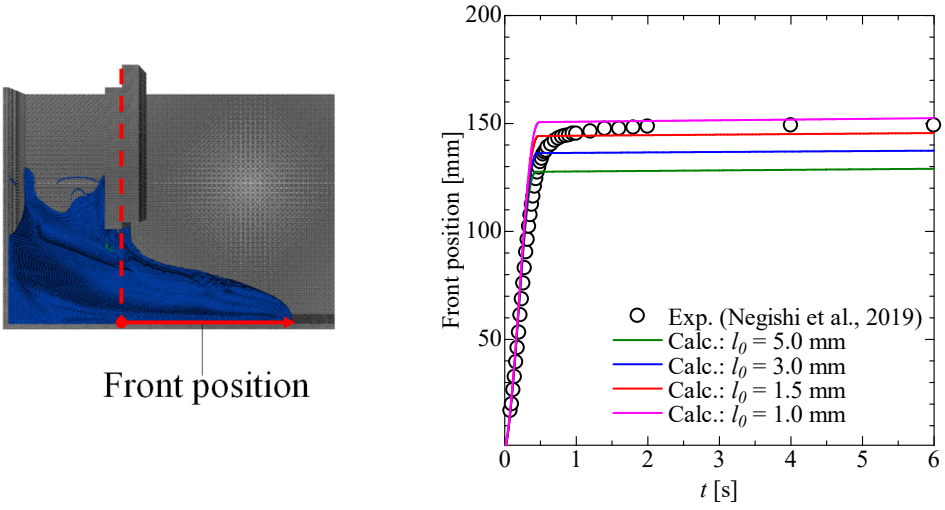

Fig. 9 Comparison of front position between experiment and calculation.

4. Conclusions

This study applied a physically consistent particle method, the Moving Particle Hydrodynamics (MPH) method (Kondo, 2021; Kondo and Matsumoto, 2021; Kondo et al., 2022), to Bingham fluid simulations by incorporating their constitutive models. To avoid the time step size restriction due to the high viscosity of Bingham fluids, the implicit velocity calculation was employed based on the weakly compressible version of the MPH method, called the MPH-WC method. Bingham fluid calculations could robustly be conducted with satisfying linear and angular momentum conservation, and the characteristic behavior of stopping and solid-like motion could be simulated.

To verify and validate the proposed method, the two-dimensional Poiseuille flow of a Bingham plastic fluid and the three-dimensional dam-break flow of a Bingham pseudoplastic fluid were calculated, and the computed results were

[DOI: 10.1299/jfst.2023jfst0035]

compared with the theoretical and experimental results. In calculating the two-dimensional Poiseuille flow of a Bingham plastic fluid, the computed velocity distribution agreed well with the theory using fine particle spacing. The computed results depended slightly on the effective radius, indicating an optimum effective radius. In calculating the three-dimensional dam-break flow of a Bingham pseudoplastic fluid, the computed free-surface behavior and history of the front position showed reasonable agreement with the experimental results, showing reasonable tendency toward convergence from the viewpoint of particle spacing. Further, the stopping behavior in the dam-break flow toward the final boot-like shape was successfully represented. It was confirmed that the proposed method promises to become a valuable approach for predicting Bingham fluids involving high viscosity and solid- and fluid-like motions.

Acknowledgements

This work was supported by the Japan Society for the Promotion of Science (JSPS) KAKENHI Grants No. 17K06137 and No. 21K03847. All the simulations in this study were performed on the JAXA Supercomputer System Generation 3 (JSS3). The authors would like to express their sincere appreciation for their support.

References

Abdolahzadeh, M., Tayebi, A. and Omidvar, P., Mixing process of two-phase non-Newtonian fluids in 2D using smoothed particle hydrodynamics, Computers and Mathematics with Applications, Vol. 78 (2019), DOI: 10.1016/j.camwa.2019.02.019.

Cao, G. and Li, Z., Numerical flow simulation of fresh concrete with viscous granular material model and smoothed particle hydrodynamics, Cement and Concrete Research, Vol. 100 (2017), DOI:10.1016/j.cemconres.2017.07.005.

Deeb, R., Kulasegaram, S. and Karihaloo, B. L., 3D modelling of the flow of self-compacting concrete with or without steel fibres. Part I: Slump flow test, Computational Particle Mechanics Vol. 1 (2014a), DOI:10.1007/s40571-014-0002-y.

Deeb, R., Kulasegaram, S. and Karihaloo, B. L., 3D modelling of the flow of self-compacting concrete with or without steel fibres. Part II: L-box test and the assessment of fibre reorientation during the flow, Computational Particle Mechanics, Vol. 1 (2014b), DOI:10.1007/s40571-014-0003-x.

de Souza Andrade, L. F., Sandim, M., Petronetto, F. and Pagliosa P., Particle-based fluids for viscous jet buckling, Computers & Graphics, Vol. 52 (2015), DOI:10.1016/j.cag.2015.07.021.

Duan, G. and Chen, B., Stability and accuracy analysis for viscous flow simulation by the moving particle semi-implicit method, Fluid Dynamics Research, Vol. 45 (2013), DOI:10.1088/0169-5983/45/3/035501.

Duan, G., Koshizuka, S. and Chen, B., A contoured continuum surface model for particle methods, Journal of Computational Physics, Vol. 298 (2015), DOI:10.1016/j.jcp.2015.06.004.

Frissane, H., Taddei, L., Lebaal, N. and Roth, S., 3D smooth particle hydrodynamics modeling for high velocity penetrating impact using GPU: application to a blunt projectile penetrating thin steel plates, Computer Methods in Applied Mechanics and Engineering, Vol. 357 (2019), DOI:10.1016/j.cma.2019.112590.

Gingold, R. A. and Monaghan, J. J., Smoothed particle hydrodynamics: theory and application to non-spherical stars, Monthly Notices of the Royal Astronomical Society, Vol. 181 No. 3 (1977), DOI:10.1093/mnras/181.3.375.

Gotoh, H. and Khayyer, A., Current achievements and future perspectives for projection-based particle methods with applications in ocean engineering, Journal of Ocean Engineering and Marine Energy, Vol. 2 (2016), DOI:10.1007/s40722-016-0049-3.

Ikari, H., Gotoh, H. and Arai, T., Numerical simulation on landslide-induced Tsunami by particle method with non-Newtonian fluid model, Journal of Japan Society of Civil Engineers, Ser. B2 (Coastal Engineering), Vol. 68, No. 2 (2012), DOI:10.2208/kaigan.68.I_66 (in Japanese).

Khayyer, A., Gotoh, H. and Shimizu, Y., Comparative study on accuracy and conservation properties of two particle regularization schemes and proposal of an optimized particle shifting scheme in ISPH context, Journal of Computational Physics, Vol. 332 (2017), DOI:10.1016/j.jcp.2016.12.005.

Kondo, M., A physically consistent particle method for incompressible fluid flow calculation, Computational Particle Mechanics, Vol. 8 (2021), DOI:10.1007/s40571-020-00313-w.

Kondo, M., Fujiwara, T., Masaie, I. and Matsumoto, J., A physically consistent particle method for high-viscous free-

surface flow calculation, Computational Particle Mechanics, Vol. 9 (2022), DOI:10.1007/s40571-021-00408-y.

Kondo, M. and Matsumoto, J., Weakly compressible particle method with physical consistency for spatially discretized system, Transactions of the Japan Society for Computational Engineering and Science, (2021), DOI:10.11421/jsces.2021.20210006 (in Japanese).

Koshizuka, S., Current achievements and future perspectives on particle simulation technologies for fluid dynamics and heat transfer, Journal of Nuclear Science and Technology, Vol. 48 (2011), DOI:10.1080/18811248.2011.9711690.

Koshizuka, S., Nobe, A. and Oka, Y., Numerical analysis of breaking waves using the moving particle semi-implicit method, International Journal for Numerical Methods in Fluids, Vol. 26 (1998), DOI:10.1002/(SICI)1097-0363(19980415)26:7<751::AID-FLD671>3.0.CO;2-C.

Koshizuka, S. and Oka, Y., Moving particle semi-implicit method for fragmentation of incompressible fluid, Nuclear Science Engineering, Vol. 123, No. 3 (1996), DOI:10.13182/NSE96-A24205.

Koshizuka, S., Shibata, K., Kondo, M. and Matsunaga, T., Moving particle semi-implicit method: a meshfree particle method for fluid dynamics, (2018), Academic Press.

Lee, B. H., Park, J. C., Kim, M. H. and Hwang, S. C., Step-by-step improvement of MPS method in simulating violent free-surface motions and impact-loads, Computer Methods in Applied Mechanics and Engineering, Vol. 200 (2011), DOI:10.1016/j.cma.2010.12.001.

Li, G., Gao, J., Wen, P., Zhao, Q., Wang, J., Yan, J. and Yamaji, A., A review on MPS method developments and applications in nuclear engineering, Computer Methods in Applied Mechanics and Engineering, Vol. 367 (2020), DOI:10.1016/j.cma.2020.113166.

Lind, S. J., Rogers, B. D. and Stansby, P. K., Review of smoothed particle hydrodynamics: towards converged Lagrangian flow modelling, Proceedings of the royal society A, No. 476 (2020), DOI:10.1098/rspa.2019.0801.

Lis: Library of Iterative Solvers for Linear Systems (online), <https://www.ssisc.org/lis/index.en.html>, (accessed on 10 September, 2023).

Liu, M. and Zhang, Z., Smoothed particle hydrodynamics (SPH) for modeling fluid-structure interactions, Science China Physics, Mechanics & Astronomy, Vol. 62, (2019), DOI:10.1007/s11433-018-9357-0.

Lucy, L. B., A numerical approach to the testing of the fission hypothesis, Astronomical Journal, Vol. 82, (1977), DOI: 10.1086/112164.

Lugt, P. M., Grease lubrication in rolling bearings, (2013), Wiley, DOI:10.1002/9781118483961.

Luo, M., Khayyer, A. and Lin, P., Particle methods in ocean and coastal engineering, Applied Ocean Research, Vol. 114 (2021), DOI:10.1016/j.apor.2021.102734.

Minatti, L. and Paris, E., A SPH model for the simulation of free surface granular flows in a dense regime, Applied Mathematical Modelling, Vol. 39, No. 1 (2015), DOI:10.1016/j.apm.2014.05.034.

Mitsoulis, E., Numerical simulation of calendaring viscoplastic fluids, Journal of Non-Newtonian Fluid Mechanics, Vol. 154, No. 2–3 (2008), DOI:10.1016/j.jnnfm.2008.03.001.

Monaghan, J. J., On the integration of the SPH equations for a highly viscous fluid, Journal of Computational Physics, Vol. 394 (2019), DOI:10.1016/j.jcp.2019.05.019.

Monaghan, J. J., SPH without a Tensile Instability, Journal of Computational Physics, Vol. 159 (2000), DOI:10.1006/jcph.2000.6439.

Morikawa, D., Asai, M., Idris, N. A., Imoto, Y. and Isshiki, M., Improvements in highly viscous fluid simulation using a fully implicit SPH method, Computational Particle Mechanics, Vol. 6 (2019), DOI:10.1007/s40571-019-00231-6.

Negishi, H., Amakawa, H., Maniwa, K., Obara, S., Hayama, M. and Dong, D., Numerical analysis of dam breaking behavior of Bingham pseudoplastic fluid by using the explicit MPS method, Transactions of the JSME (in Japanese), Vol. 85, No. 875 (2019), DOI:10.1299/transjsme.19-00086.

Negishi, H., Kondo, M., Amakawa, H., Obara, S. and Kurose, R., A fluid lubrication analysis including negative pressure using a physical consistent particle method, Computational Particle Mechanics, (2023), DOI:10.1007/s40571-023-00584-z.

Nishida, A., Experience in developing an open source scalable software infrastructure in Japan, Computer Science and Its Applications -ICCSA 2010, Lecture Notes in Computer Science, Springer, Vol. 6017 (2010), DOI:10.1007/978-3-642-12165-4_36.

Pan, W., Tartakovsky, A. M. and Monaghan, J. J., Smoothed particle hydrodynamics non-Newtonian model for ice-sheet and ice-shelf dynamics, Journal of Computational Physics, Vol. 242 (2013), DOI:10.1016/j.jcp.2012.10.027.

[DOI: 10.1299/jfst.2023jfst0035]

Papanastasiou, T. C., Flows of materials with yield, Journal of Rheology, Vol. 31, No. 5 (1987), DOI:10.1122/1.549926.

Ren, J., Jiang, T., Lu, W. and Li, G., An improved parallel SPH approach to solve 3D transient generalized Newtonian free surface flows, Computer Physics Communications, Vol. 205 (2016), DOI:10.1016/j.cpc.2016.04.014.

Ren, J, Ouyang, J., Jiang, T. and Li, Q., Simulation of complex filling process based on the generalized Newtonian fluid model using a corrected SPH scheme, Computational Mechanics, Vol. 49 (2012), DOI:10.1007/s00466-011-0669-3.

Rossi, E., Garcia de Beristain, I., Vazquez-Quesada, A., López-Aguilar, J. E. and Ellero, M., SPH simulations of thixo-viscoplastic fluid flow past a cylinder, Journal of Non-Newtonian Fluid Mechanics, Vol. 308 (2022), DOI:10.1016/j.jnnfm.2022.104891.

Russell, M. A., Souto-Iglesias, A. and Zhodi, T. I., Numerical simulation of laser fusion additive manufacturing processes using the SPH method, Computer Methods in Applied Mechanics and Engineering, Vol. 341 (2018), DOI:10.1016/j.cma.2018.06.033.

Saito, Y., Kato, M., Otsuki, M., Kimura, I., Shimizu, Y. and Isenko, E., Refinement of MPS method for practical application to snow avalanches, Annals of Glaciology, Vol. 53, No. 61 (2012), DOI:10.3189/2012AoG61A014.

Shadloo, M. S., Oger, G. and Touze, D. L., Smoothed particle hydrodynamics method for fluid flows, towards industrial applications: Motivations, current state and challenges, Computers and Fluids, Vol. 136 (2016), DOI: 10.1016/j.compfluid.2016.05.029.

Shao, S. and Lo, E. Y. M., Incompressible SPH method for simulating Newtonian and non-Newtonian flows with a free surface, Advances in Water Resources, Vol. 26, No. 7 (2003), DOI:10.1016/S0309-1708(03)00030-7.

Shao, S. and Lo, E. Y. M., Incompressible SPH method for simulating Newtonian and non-Newtonian flows with a free surface, Advances in Water Resources, Vol. 26, No. 7 (2003), DOI:10.1016/S0309-1708(03)00030-7.

Takahashi, T., Dobashi, Y., Fujishiro, I., Nishita, T. and Lin, M., Implicit formulation for SPH-based viscous fluids, Computer Graphics Forum, Vol. 34 (2015), DOI:10.1111/cgf.12578.

Tao, Y., Shibata, K. and Koshizuka, S., A Bingham snow model for train safety built using the moving particle semi-implicit method, Transaction of JSCES, (2017), DOI:10.11421/jsces.2017.20170010.

Violeau, D. and Issa, R., Numerical modelling of complex turbulent free-surface flows with the SPH method: an overview, International Journal for numerical methods in fluids, Vol. 53 (2007), DOI:10.1002/fld.1292.

Violeau, D. and Rogers, B. D., Smoothed particle hydrodynamics (SPH) for free-surface flows: past, present and future, Journal of Hydraulic Research, Vol. 54 (2016), DOI:10.1080/00221686.2015.1119209.

Wang, Z. B., Chen, R., Wang, H., Liao, Q., Zhu, X. and Li, S. Z., An overview of smoothed particle hydrodynamics for simulating multiphase flow, Applied Mathematical Modelling, Vol. 40 (2016), DOI:10.1016/j.apm.2016.06.030.

Weiler, M., Koschier, D., Brand, M. and Bender, J., A physically consistent implicit viscosity solver for SPH fluids, Computer Graphics Forum, Vol. 37 (2018), DOI:10.1111/cgf.13349.

Xenakis, A. M., Lind, S. J., Stansby, P. K. and Rogers, B. D., An incompressible SPH scheme with improved pressure predictions for free-surface generalized Newtonian flows, Journal of Non-Newtonian Fluid Mechanics, Vol. 218 (2015), DOI:10.1016/j.jnnfm.2015.01.006.

Xie, F., Zhao, W. and Wan, D., Overview of moving particle semi-implicit techniques for hydrodynamic problems in ocean Engineering, Journal of Marine Science and Application, Vol. 21 (2022), DOI:10.1007/s11804-022-00284-9.

Xie, J. and Jin, Y. C., Parameter determination for the Cross rheology equation and its application to modeling non-Newtonian flows using the WC-MPS method, Engineering Applications of Computational Fluid Mechanics, Vol. 10, No. 1 (2016), DOI:10.1080/19942060.2015.1104267.

Xu, R., Stansby, P. and Laurence, D., Accuracy and stability in incompressible SPH (ISPH) based on the projection method and a new approach, Journal of Computational Physics, Vol. 228 (2009), DOI:10.1016/j.jcp.2009.05.032.

Xu, T. and Jin, Y. C., Modeling free-surface flows of granular column collapses using a mesh-free method, Powder Technology, Vol. 291 (2016), DOI:10.1016/j.powtec.2015.12.005.

Xu, X. and Deng, X. L., An improved weakly compressible SPH method for simulating free surface flows of viscous and viscoelastic fluids, Computer Physics Communications, Vol. 201 (2016), DOI:10.1016/j.cpc.2015.12.016.

Xu, X., Ouyang, J., Yang, B. and Liu, Z., SPH simulations of three-dimensional non-Newtonian free surface flows, Computer Methods in Applied Mechanics and Engineering, Vol. 256 (2013), DOI:10.1016/j.cma.2012.12.017.

Xu, Z. and Li, Z., Numerical method for predicting flow and segregation behaviors of fresh concrete, Cement and Concrete Composites, Vol. 123 (2021), DOI:10.1016/j.cemconcomp.2021.104150.

[DOI: 10.1299/jfst.2023jfst0035]

Xu, Z., Li, Z. and Jiang, F., The applicability of SPH and MPS methods to numerical flow simulation of fresh cementitious materials, Construction and Building Materials, Vol. 274 (2021), DOI:10.1016/j.conbuildmat.2020.121736.

Xu, Z., Li, Z. and Jiang, F., Numerical approach to pipe flow of fresh concrete based on MPS method, Cement and Concrete Research, Vol. 152 (2022), DOI:10.1016/j.cemconres.2021.106679.

Ye, T., Pan, D., Huang, C. and Liu, M., Smoothed particle hydrodynamics (SPH) for complex fluid flows: recent developments in methodology and applications, Physics of Fluid, Vol. 31 (2019), DOI:10.1063/1.5068697.

Zago, V., Bilotta, G., Hérault, A., Dalrymple, R. A., Fortuna, L., Cappello, A., Ganci, G. and Del Negro, C., Semi-implicit 3D SPH on GPU for lava flows, Journal of Computational Physics, Vol. 375 (2018), DOI:10.1016/j.jcp.2018.07.060.

Zhu, H., Martys, N. S., Ferraris, C. and De Kee, D., A numerical study of the flow of Bingham-like fluids in two-dimensional vane and cylinder rheometers using a smoothed particle hydrodynamics (SPH) based method, Journal of Non-Newtonian Fluid Mechanics, Vol. 165 (2010), DOI:10.1016/j.jnnfm.2010.01.012.

Zhou, G., Ge, W. and Li, J., Smoothed particles as a non-Newtonian fluid: A case study in Couette flow, Chemical Engineering Science, Vol. 65 (2010), DOI:10.1016/j.ces.2009.12.020.

[DOI: 10.1299/jfst.2023jfst0035]